

PACS numbers: 42.55.Rz; 42.60.Jf; 42.15.Dp
DOI: 10.1070/QE2010v040n04ABEH014061

Shack – Hartmann wavefront sensor for measuring the parameters of high-power pulsed solid-state lasers*

A.G. Aleksandrov, V.E. Zavalova, A.V. Kudryashov, A.L. Rukosuev, P.N. Romanov, V.V. Samarkin, Yu.V. Sheldakova

***Abstract*. The wavefront of the radiation of two types from high-power solid-state (Ti : sapphire and Nd : glass) lasers is experimentally studied. The measurements are performed using a Shack – Hartmann wavefront sensor. The technical and functional potential of this sensor in measuring laser-based schemes is demonstrated. The results of measuring both static and dynamic wavefront aberrations are discussed. The estimated dynamics of defocus aberration is in agreement with the experimental data.**

Keywords: *Shack – Hartmann wavefront sensor, solid-state lasers, measurement of wavefront aberrations, radiation quality, adaptive optical system with feedback for wavefront correction.*

1. Introduction

The study of the radiation wavefront for high-power pulsed solid-state lasers is an urgent problem, because it helps to advance in the laser design and improve the laser radiation characteristics. Lasers of this type, characterised by a petawatt power and ultrashort pulse width, make it possible to solve modern problems of basic research in the field of interaction of superstrong (exceeding intraatomic) electromagnetic fields with matter. In particular, these are problems of thermonuclear fusion, atomic and relativistic physics, astrophysics, and even medicine. Projects of many countries, including 'National Ignition Facility' (the United States), 'Laser Megajoule' (France), 'Extreme Light Infrastructure' (European Union), 'Shenguang' (China), and 'Ray' (the Russian Federation) are aimed at developing such systems. Great progress has been made in this field in the last decade. Modern 800-nm femtosecond Ti : sapphire lasers have a power of several hundreds of terawatts and a peak focused-beam intensity of 10^{22} W cm^{-2} [1]. The latest models of 1053-nm Nd : glass lasers have an output energy of several megajoules per pulse [2]. The general tendency in the further development of these systems is to focus the laser radiation into a spot with a size close to the diffraction limit, which can be done by only eliminating wavefront distortions.

We have gained some experience in measuring and correcting radiation wavefronts in the above-mentioned laser systems [3 – 7] at many well-known laboratories and institutes in different countries (LULI, Ecole Polytechnique, Palaiseau, France; project FIREX Laser, Osaka University, Japan; project PHELIX Laser, Center for Heavy Ion Research (GSI), Darmstadt, Germany; project ATLAS, Max Planck Institute, Garching, Germany; project ALLS, National Research Institute, Varrenes, Canada; project TRIDENT Laser, Los Alamos National Laboratory, the United States; project Helen, AWE, Aldermaston, England; Institute of Physics, Beijing, China; etc.). In this paper, we report the results of some experimental studies carried out with a Shack – Hartmann sensor.

2. Principle of wavefront measurement with a Shack – Hartmann sensor and application of this sensor in laser systems

The Shack – Hartmann sensor was chosen to measure the radiation characteristics of the lasers under consideration because of its advantages over other sensors, including interferometric ones. The main advantages of this sensor include the wide spectral range of operation for both cw and pulsed radiation and low sensitivity to mechanical vibrations. An important feature of this sensor is the possibility of obtaining quantitative information on the wavefront phase and intensity distribution in the near and far field simultaneously, which allows one to estimate the radiation quality parameter M^2. The principle of sensor operation, methods of phase reconstruction, and the problems that can be solved using this sensor were reported in many publications (see, for example, [8 – 16]). The Shack – Hartmann method is based on measuring the local slopes of individual wavefront portions, into which the arriving front is divided by a Hartmann mask (in our case, a microlens raster, i.e., a glass plate with a microrelief formed by an array of microlenses several hundreds of micrometers in size). We apply the algorithm of wavefront reconstruction that is based on modal phase expansion [14], using the least-squares method for determining the Zernike coefficients. It is especially convenient to express the phase as a sum of Zernike polynomials because of the physical meaning of this representation: it takes into account all types of wavefront aberrations. In addition, there are formulas for recalculating the Zernike coefficients into classical Seidel aberrations, which are traditionally used in optical measurements.

*Reported at the conference 'Laser Optics 2008', St. Petersburg, Russia.

A.G. Aleksandrov, V.E. Zavalova, A.V. Kudryashov, A.L. Rukosuev, P.N. Romanov, V.V. Samarkin, Yu.V. Sheldakova Moscow State Open University, Shatura Branch, ul. Moscowskaya 10, 140700 Shatura, Moscow region, Russia; e-mail: vzavalova@nightn.ru

Received 28 January 2009; revision received 4 January 2010
Kvantovaya Elektronika **40** (4) 321 – 326 (2010)
Translated by Yu.P. Sin'kov

The radiation intensity distribution over the beam aperture is reconstructed from the analysis of the Hartmann pattern, which is an array of spots on a CCD matrix, with discrete intensity values in each spot pixel. A polynomial approximation is also used to construct this distribution. After determining the phase and intensity distributions in the lens raster plane (near field), one can calculate the intensity distribution in the lens focus (far field), and, therefore, the radiation quality parameter M^2. The calculations are based on the relations determined in the ISO/DIS 11146 standard [17]. Applying them to our case, we can calculate the quality parameter as the ratio of the far-field beam diameter d_f, calculated from the measured phase and radiation intensity distributions, to the similar diameter d_f^G of a Gaussian beam with a plane wavefront: $M^2 = d_f/d_f^G$. A device for measuring the radiation quality parameter by this method was described in [18].

The accuracy of the wavefront measurement using a Shack–Hartmann sensor is proportional to the minimum measured wavefront slope S_{min}/f_L, where f_L is the microlens focal length and S_{min} is the minimum spot displacement, related to the accuracy in determining the centres of spots in the Hartmann pattern. A statistical analysis of the probability density distribution for the error caused by the image discretization was performed in a model Monte Carlo experiment. The centres of spots and their displacements were set. The new centre positions were determined from the first moments of the intensity distributions, which has 255 gradation levels for a 8-bit camera, on the pixel (discrete) spot structure. The thus obtained probability density distribution for the measurement error is shown in Fig. 1. About 90 % of the area under the distribution corresponds to the error range $\sigma < 0.1$ of a pixel; thus, we can conclude that the error in determining the spot centre position (or, which is the same, the minimum spot displacement) corresponds to 0.1 pixel.

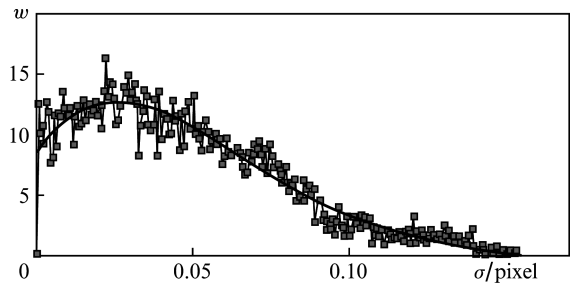

Figure 1. Distribution of the probability density w of the error σ in the calculation of the spot centre position. The solid line is an approximation.

Concerning the microlens parameters, the Fresnel number [more specifically, the ratio $d_L/(f_L\lambda/d_L)$, where d_L is the microlens diameter] must be controlled to increase the phase measurement accuracy. The microlens raster is valid for measurements when $N_F > 1$. In this case, the dynamic range of spot displacement in the region under study is proportional to $(0.5d_L - R_d)/f_L$, where $R_d = 1.22f_L\lambda/d_L$ is the spot diffraction radius. The dynamic range widens with an increase in d_L and a decrease in f_L, while the phase measurement accuracy decreases.

In practice, to perform wavefront measurements, one must match the beam and CCD matrix detector apertures. When the wavefront must be measured at a specific point, a telescopic system is applied, which conjugates the planes of the object measured and its image on the microlens raster.

A number of problems are successfully solved using a Shack–Hartmann wavefront sensor. Primarily, this is the testing of active laser elements and determination of their optical quality, as well as the presence of defects. Rough violations of crystal homogeneity in the form of striations manifest themselves in the Hartmann pattern as spot splitting. If the aberrations exceed the tolerance limit, they must be replaced. Another problem is the alignment of optical elements along the beam axis. The amplitudes of the low-order aberrations (defocus, astigmatism, coma, spherical aberration), caused by poor alignment, can be minimised based on measurements in the operating regime. The measurements of the laser radiation wavefront in both cw and pulsed regimes are of particular interest. Some examples are given in Section 3. All these data are necessary for constructing adaptive optical systems (AOSs) with feedback for correcting the wavefront distortions; the measurement error should be smaller than the AOS error. An optimal corrector is prepared based on the results of these measurements, and an algorithm for controlling its surface is developed proceeding from the phase conjugation of the surface with the measured laser radiation wavefront. The radiation intensity in the focus can be estimated as $I = \varepsilon/(\tau S)$, where ε is the energy per pulse, τ is the pulse width, and S is the beam area in the focal plane. The focal spot (area S) can be reduced for high-quality beams by eliminating wavefront distortions. The minimum size of the focal spot corresponds to the first diffraction radius.

3. Application of wavefront sensor in measuring schemes

3.1 Measurements of the Ti : sapphire laser radiation wavefront

Depending on the problems stated, the Shack–Hartmann wavefront sensor can measure the beam characteristics prac-tically at any point of the laser optical system. Typically, AOS measurements are performed at the end of the optical channel (after the compressor, which is located before the interaction chamber, where the laser radiation is focused on the target). The sensor is always located after the corrector.

The measurement results obtained at the Institute of Physics (Beijing, China) for a Ti : sapphire laser (pulse energy 0.6 J, pulse width 50 fs, and output beam diameter 50 mm) are shown in Fig. 2. An additional vacuum chamber was placed between the interaction chamber and compressor to mount a corrector and rotational mirrors. After reflecting from the adaptive mirror, the laser radiation mostly passed to the target, while the rest arrived to the measuring arm through the output glass window of the chamber. The optical distortions of the elements, including the filters attenuating the radiation power to the safe level for the CCD matrix, were monitored by the sensor. This made it possible to minimise the contribution of introduced distortions. The measurements showed that the main beam aberrations were defocus and astigmatism. The beam intensity distribution in the long-focal-length lens focus was monitored by an independent radiation analyser. The lens was located before

the interaction chamber in the measuring channel. The measured intensity was compared with the calculation result based on the Shack – Hartmann measurements.

Figure 2a presents a table of measured aberrations and the interference pattern without the defocus aberration, reconstructed from the Hartmann pattern. The calculated and measured intensity distributions in the focus are shown in Figs 2b and 2c. It can be seen that the calculated intensity in the focus is in agreement with the measured value and that the improvement of the laser radiation quality, which leads to a decrease in the focal spot size (Fig. 2d), is the result of the elimination of wavefront aberrations (mainly astigmatism) by the adaptive system.

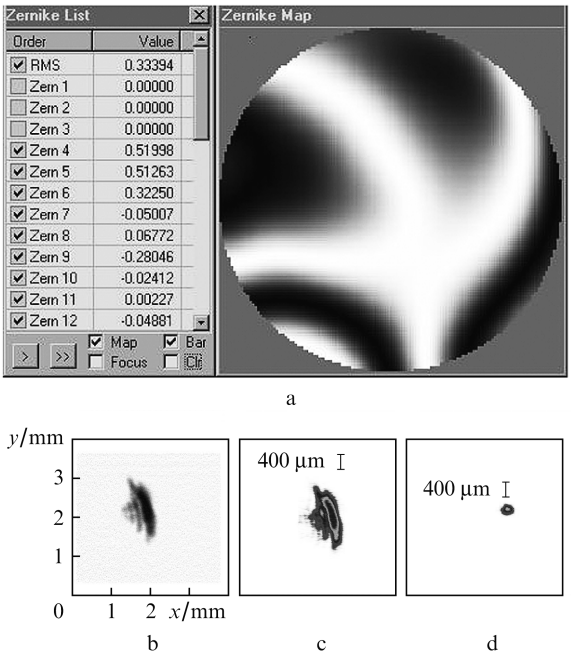

Figure 2. (a) Interference pattern of the measured wavefront and the (b) calculated and (c, d) measured intensity distributions for Ti : sapphire laser radiation in the focus of a 5-m focal length lens (the measurements were performed (c) before and (d) after correcting the wavefront distortions, disregarding defocus). The standard deviations (RMS) for the change in phase and the Zernike coefficients (in micrometers) are listed in the left top corner.

However, there are measurements indicating that in some cases the desired result cannot be achieved because of the residual (uncorrelated by the adaptive system) aberrations produced by the focusing optics. An example is the experiments performed at the Quebec University (Canada) [5] with a Ti : sapphire laser (power 10 TW, pulse width 25 fs, repetition frequency 10 Hz). The wavefront aberrations were first measured by the sensor before the target chamber entrance. The laser beam was focused on the target by a parabolic mirror. The sensor was included in the adaptive scheme of radiation wavefront correction.

The correction result was monitored by the CCD matrix, onto which the image of the focal spot on the target was transferred. The adaptive system almost completely eliminated the beam distortions, whereas the decrease in the focal spot area on the target was insufficient. Then the optical scheme was rearranged. The sensor was installed behind the target chamber, which made it possible to measure directly the beam behind the focusing parabolic mirror. Now, due to the correction, the focal spot on the target decreased in size from 8.6×14.8 μm to 5×4 μm, which provided a peak intensity of 3×10^{20} W cm^{-2} [5].Thus, the focusing parabolic mirror was found to introduce an astigmatism with an amplitude of $\sim 3\lambda$, which could not be completely eliminated by aligning.

3.2 Study of the wavefront aberrations for a high-power Nd : glass laser

Typical optical schemes of extremely high-power Nd:glass lasers have a long optical channel, which includes special functional elements. Schematically, they can be presented as individual blocks, amplifiers and spatial filters, which transmit radiation from the oscillator and preamplifier. Multiple transmission of radiation through the amplifiers is generally used. The possibility of obtaining extremely high-power single pulses with a megajoule energy is characteristic of the lasers of this type. The interval between such pulses can be as long as several hours. We report here some generalised results and characteristic dependences, obtained by measuring the radiation parameters of modern Nd : glass lasers with a pulse energy of several kilojoules and pulse width of several nanoseconds.

The radiation wavefront of such lasers is generally investigated at two main stages. At the first stage measurements are performed, and the aberrations introduced by the transmission channel are analysed. The master oscillator or a probe laser are used as probe radiation sources. The aberrations measured at this stage are static and do not contain any contributions from nonlinear effects; their sum is a superposition of the distortions introduced by individual elements. It is impossible to completely eliminate the wavefront distortions of this type; however, they can be minimised by a more exact alignment or choosing higher quality optical elements. This stage is important from the technical point of view but is generally of no scientific interest.The wavefront recorded in such measurements is thereafter often used as a reference when studying the laser beam wavefront aberrations arising in the operating regime. At the second stage the dynamic aberrations of the laser beam wavefront, which are formed during lasing, are analysed [19].

Here is an example of typical temporal dynamics of radiation wavefront for a pulsed laser with an energy of no less than 1 J per pulse. To select the pump-induced aberrations, the calculations were performed for the wavefront measured before the pump pulse and including static aberrations. The data were recorded and processed immediately after the pump pulse and stopped when their distributions became steady-state (with deviations no larger than the measurement error). Figure 3 shows the typical behaviour of individual wavefront aberrations (expressed in terms of Zernike coefficients) after the pump pulse. The defocus introduced by the thermal lens (induced by the thermal action of active-element pumping) makes a large contribution to these distortions. The induced thermal lens leads also to some other aberrations that are typical of thick lenses; however, they are several times smaller.

Three main stages can be selected in the defocus dynamics. First, during a relatively short (several seconds) time interval the radiation defocusing reaches a maximum. At this stage the role of the kinetic nonequilibrium processes (related in particular to the thermal relaxation) in the

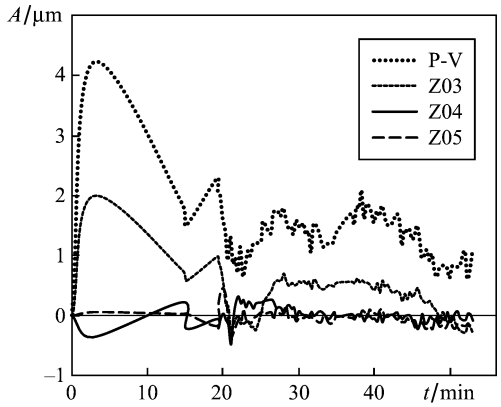

Figure 3. Wavefront aberration dynamics after an Nd : glass-laser pulse: (Z03) defocus; (Z04, Z05) second-order astigmatism along the $0 - \pi/2$ and $0 \pm \pi/4$ axes, respectively (in the form of Zernike coefficients); and P-V values.

internal energy balance is fairly high. Then the defocusing significantly decreases for several minutes, because the mechanisms of heat removal from the active element are involved. After the defocus drop from the maximum value the amplitudes of all aberrations and the P-V value (the sum of aberrations for the phase expansion up to 36 terms) first oscillate near a quasi-stationary value for a long time and then begin to decrease, as the thermodynamic equilibrium between the active element and cooling flow is established. These (slower) processes take no less than an hour.

After the defocus, the next in magnitude are the second- and third-order astigmatisms. Their initial amplitudes are several times smaller, and decay occurs for a shorter time. The spatial inhomogeneity of active-element pumping is known to be the main cause of astigmatism. Thus, the largest changes in aberrations (and P-V) occur during the first several minutes immediately after pumping.

To estimate how the aberrations of Nd : glass laser radiation change in time, we will construct a simplified thermophysical model. In high-power lasers the active elements, located in amplification stages, are thick disks with large diameters D (~ 20 cm) and thicknesses $h \ll D$. The active elements are pumped from faces ($r = D/2$) in the direction r, which is perpendicular to the laser beam propagation direction (axis x), while cooling occurs from the lateral disk surfaces (at $x = \pm h/2$), as a result of which the disks are heated and an axisymmetric (parabolic) temperature profile arises. Since the optical properties of a medium are characterised by its refractive index n, and a change in n is proportional to temperature change [20], the expression for the total differential $\mathrm{d}n = (\partial n/\partial T)\mathrm{d}T$ (where $\mathrm{d}T$ is a temperature change and $\partial n/\partial T$ is the thermooptical coefficient) describes a thermal lens. The details of the theory containing its properties for solid-state lasers can be found in many publications (see, for example, [21, 22]).

Under steady-state conditions a thermal lens defocuses radiation; it can easily be eliminated and, therefore, is not a serious problem. In pulsed lasers the thermal-lens properties significantlyly change with time and affect radiation focusing on the target. As was mentioned above, the thermal lens is caused by temperature distribution; therefore, the change in the defocus aberration will be considered by solving the time-dependent heat-conduction problem. After pumping the active element is cooled due to the thermal conduction and heat transfer from its surface (the latter is performed by a gas flow with a temperature T_g). The disk thickness is much smaller than the radius; therefore, to solve analytically the time-dependent heat-conduction equation, we will use the thin-plate model. The initial condition is the temperature distribution established after the pumping. Although the temperature $T(r_n)$ is parabolically distributed along the disk radius, it can be considered constant and independent of the transverse coordinate x at any point $r = r_n$. The boundary conditions were as follows: on the plate axis, at $x = 0$ (in the central cross section of the disk), in view of the axial symmetry, $\partial T/\partial x|_{x=0} = 0$, while on the plate surface

$$\left.\frac{\partial T}{\partial x}\right|_{x=\pm\delta} = -\frac{\alpha}{k}(T - T_\mathrm{g}),$$

where α is the heat transfer coefficient, k is the thermal conductivity, and $\delta = \pm h/2$. The solution to this time-dependent problem can generally be represented as the series

$$\Theta = \sum_{n=1}^{\infty} \frac{2\sin\mu_n}{\mu_n + \sin\mu_n\cos\mu_n}\cos(\mu_n X)\exp(-\mu_n^2 F), \qquad (1)$$

where $\Theta = \Delta T(\tau, 0)/\Delta T(0, 0)$ is the dimensionless temperature, $\Delta T(0, 0)$ is the initial difference between the temperature on the axis (at $\tau = 0$) and the ambient temperature T_g, $X = x/\delta$ is the dimensionless coordinate, $F = a\tau/\delta^2$ is the Fourier number (dimensionless time), $a = k/(\rho c_p)$ is the thermal diffusivity, ρ is the density, and c_p is the specific heat. The μ value is determined from the characteristic equation $\cot\mu = \mu/\mathrm{Bi}$, obtained by substituting the boundary conditions into the quasi-one-dimensional heat-conduction equation. The characteristic equation has a set of solutions μ_n, which are determined by the dimensionless number $\mathrm{Bi} = \alpha\delta/k$. This parameter describes the relationship between the temperature in a solid and the heat transfer conditions on its surface.

The solution for cooling solids of finite size showed that at short times the rate of change in temperature at individual points of the solid depends on the initial temperature distribution. With an increase in time the disordered cooling stage is transformed into a regular stage, in which the expansion terms rapidly decrease, and the initial temperature distribution ceases to play any significant role; therefore, the process is completely determined by only the heat transfer conditions on the solid surface and the thermal and physical properties and the size of the solid. The estimation will be based on the fact that series (1) is convergent; thus, at $F > 0.3$ we can restrict ourselves to the first expansion term. Then the cooling on the axis ($X = 0$) can approximately be described by the expression

$$\Theta = \exp\left(-\mu_1^2\frac{a\tau}{\delta^2}\right), \qquad (2)$$

where the first root $\mu_1 \approx \sqrt{\mathrm{Bi}}$. Formula (2) can be used to roughly estimate the decay increment or the active-element cooling rate:

$$\tau_\mathrm{inc}^{-1} = \frac{2\alpha a}{k\delta}. \qquad (3)$$

We choose the following thermal and physical parameters of the active element: density $\rho = 2\times10^3$ kg m^{-3}, specific heat $c_p = 0.67$ kJ kg^{-1} K^{-1}, thermal conductivity $k = 0.74$ W m^{-1} K^{-1}, and heat transfer coefficient $\alpha \simeq 10$ W m^{-2} K^{-1} (the latter parameter characterises the convective gas cooling). Thus, substituting the numerical data into (2), we find that Θ decreases by a factor of e after about 15 min. Cooling to a constant temperature (accurate to 10 %) requires a time $t = -\tau_{\text{inc}} \ln 0.1$ (52 min for the above-mentioned parameters).

The theoretically estimated time of active-element cooling within the above-described model is in agreement with the experimental value (Fig. 3). This estimate allows one to determine the time interval between pulses at which the effect of the active medium on the next pulse is minimum.

In constructing the algorithm for correcting wavefront aberrations in adaptive systems with a closed feedback, another very important factor is the pulse-to-pulse reproducibility of aberrations. Figure 4 shows a typical change in aberrations in laser AOSs. One can see that before the beginning of each following pulse the pump-induced processes in the laser active medium relax. In this case, the difference in the wavefronts for the nearest pulses has a fluctuation character and gives a standard deviation of the phase change (RMS = 0.1λ) close to the measurement error.

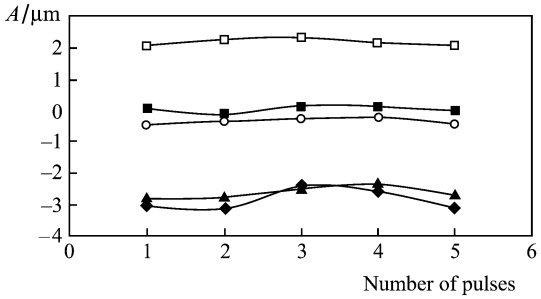

Figure 4. Changes in the amplitudes of wavefront aberrations for single Nd : glass-laser pulses: (◆) defocus, (□) astigmatism (0), (▲) astigmatism (45°), (○) coma along the x axis, and (■) spherical aberration.

However, it should be noted that in some cases the difference in the wavefronts of neighboring pulses is large, and it is rather difficult to find any pulse-to-pulse correlation between aberration amplitudes. If an adequate algorithm for controlling the adaptive system cannot be found, the radiation quality is improved by correcting static aberrations. An example is the situation that occurred at the AWE Laboratory (England) when the radiation of a lamp-pumped Nd : glass laser (pulse width 100 ps, energy up to 1 kJ per pulse) was corrected. The wavefront sensor was located behind the four-pass amplifier, before the focusing optics. The defocus and astigmatism aberrations accumulated with an increase in their amplitudes from pulse to pulse.

4. Conclusions

It was shown that the Shack–Hartmann wavefront sensor is a multifunctional device for measuring the radiation of high-power (Ti : sapphire and Nd : glass) lasers, which allows one to do the following:

(i) simultaneously measure the phase and intensity, determine the aberrations affecting the radiation quality, and calculate the radiation quality parameter;

(ii) investigate the wavefront aberrations related to both the quality and alignment of optical elements and minimise these aberrations in real time in any part of the optical laser system;

(iii) investigate the aberrations caused by the inhomogeneity of active-element refractive index and separate those related to the primary defects of the elements from the aberrations due to the nonlinear effects induced by pumping of the active medium (in particular, thermal lens);

(iv) experimentally study the aberration dynamics.

The results of studying the thermal-lens behaviour after the pump pulse are in agreement with the estimates obtained by solving the model time-dependent heat conduction problem. The estimates found make it possible to determine the allowable interval between pulses as a function of the thermophysical properties of the active element, its geometrical size, and the heat transfer conditions on its surface. This information is important for developing an operation algorithm for adaptive systems with feedback

Thus, the above-described measurements facilitate the solution of the main problem: attainment of radiation intensity distribution in the focus close to the diffraction limit.

References

1. Bahk S.-W.G., Rousseau P., Planchon T.A., et al. *Opt. Lett.*, **29**, 24 (2004).
2. Wegner P.J., Auerbach J.M., Bowers M.W., et al. *Appl. Opt.*, **46**, 16 (2007).
3. Kudryashov A., Alexandrov A., Zavalova V., Rukosuev A., Samarkin V. *Proc. SPIE Int. Soc. Opt. Eng.*, **6346**, 634 (2007).
4. Aleksandrov A.G., Zavalova V.E., Kudryashov A.V., Rukosuev A.L., Samarkin V.V. *Zh. Prikl. Spektrosk.,* **72**, 5 (2005).
5. Fourmaux S., Payeur S., Martin F., Ozaki T., Kieffer J.C., Alexandrov A., Kudryashov A. *Proc. 7th Int. Workshop on Adaptive Optics for Industry and Medicine* (Shatura, 2009) pp 108 – 109.
6. Aleksandrov A.G., Zavalova V.E., Kudryashov A.V., Rukosuev A.L., Romanov P.N., Samarkin V.V. *Opt. Zh.,* **71**, 11 (2004).
7. Wattellier B., Fuchs J., Zou J.P., Kudryashov A., Aleksandrov A., et al. *J. Opt. Soc. Am. B*, **20**, 8 (2003).
8. Taranenko V.G., Shanin O.I. *Adaptivnaya optika* (Adaptive Optics) (Moscow: Radio i Svyaz', 1990).
9. Malacara D. (Ed.) *Optical Shop Testing* (New York: Wiley, 1978; Moscow: Mashinostroenie, 1985).
10. Roggemann M.C., Schultz T.J., Ngai C.W. *J. Appl. Opt.*, **32**, 38 (1999).
11. Yoon G.Yo., Jitsuno T., Nakatsuka M., Nakai S. *Appl. Opt.*, **1**, 35 (1996).
12. Irwan R., Lane R.G. *Appl. Opt.*, **32**, 38 (1999).
13. Liang J., Grimm B., Goelz S., Bille J.F. *Opt. Soc. Am. A*, **7**, 11 (1994).
14. Southwell W.H. *J. Opt. Soc. Am.*, **8**, 70 (1980).
15. Noll R. *J. Opt. Soc. Am.*, **3**, 66 (1976).
16. Zavalova V.Ye., Kudryashov A.V. *Proc. SPIE Int. Opt. Soc. Eng.*, **4493**, 277 (2002).
17. Test Method for Laser Beam Parameters: Beam Width, Divergence Angle and Beam Propagation Factor. Document ISO/DIS 11146 (1996).
18. RF Patent 58702, priority of May 30, 2007.
19. Wattellier B., Fuchs J., Zou J.P., Abdeli K., Pépin H., Haefner C. *Opt. Lett.*, **29**, 21 (2004).

20. Born M., Wolf E. *Principles of Optics* (Oxford: Pergamon, 1969; Moscow: Nauka, 1969).
21. Zverev G.M., Golyaev Yu.D., Shalaev E.A., Shokin A.A. *Lazery na alyumoittrievom granate s neodimom* (Nd : YAG Lasers) (Moscow: Radio i Svyaz', 1985).
22. Graf Th., Weber R., Schmid M., Weber H.P. *Proc. 2nd Int. Workshop on Adaptive Optics for Industry and Medicine* (Durham, England, 1999).